PROCEEDINGS, TOUGH Symposium 2006
Lawrence Berkeley National Laboratory, Berkeley, California, May 15–17, 2006

VALIDATION OF THE ACTIVE FRACTURE MODEL FOR UNSATURATED FRACTURE FLOW USING NUMERICAL EXPERIMENTS

Quanlin Zhou
ETIC Engineering Inc., Oakland, CA 94612
e-mail: qzhou@eticeng.com

ABSTRACT

The active fracture model has been successfully applied to modeling unsaturated flow and transport in fractured rock at Yucca Mountain, Nevada. It accounts for complex flow features (e.g., preferential flow) observed in the field in a relatively large scale model (Liu et al., 1998). In this model, the effects of active, water-conducting fractures on effective liquid saturation (S_e), capillary pressure (P_c), relative permeability (k_r), and fracture-matrix interface area are taken into account in the framework of the van Genuchten constitutive equations, with an additional parameter (γ) introduced to represent fraction of active fractures. This parameter is often obtained through model calibration. However, a direct relationship between the magnitude of γ and the fractured-rock characteristics has not been achieved so far. Our paper aims at demonstrating (1) whether the effective $k_r^a - P_c^a - S_e^a$ relationships in the active fracture model can be reproduced using numerical experiments, and (2) whether the γ parameter can be linked to the spatial variabilities of fracture geometric and hydraulic properties. The numerical experiments were conducted in four steps: (1) generating random fields of log fracture permeability, with varying correlation lengths and standard deviations; (2) simulating steady-state unsaturated flow in fractured rock using TOUGH2; (3) upscaling effective, flux-weighted $\overline{S_e}$, $\overline{P_c}$, $\overline{k_r}$ values for the entire flow system; and (4) deriving the effective $\overline{k_r^a} - \overline{P_c^a} - \overline{S_e^a}$ constitutive relationships with the $\overline{S_e^a}$ values varying with specified top boundary conditions. Our results indicate that (1) the effective $\overline{k_r^a} - \overline{P_c^a} - \overline{S_e^a}$ relationships are different from the local-scale, homogeneous $k_r - P_c - S_e$ ones, indicating the effects of active fractures with high flow rates, (2) such difference increases with increasing degree of heterogeneity, and (3) the γ parameter increases with increasing degree of fracture-permeability heterogeneity, and (4) it changes with $\overline{S_e^a}$, which is different from the constant-value assumption usually established in the active fracture model.

1. INTRODUCTION

The active fracture model was developed by Liu et al. (1998) to effectively account for unsaturated flow and transport features in naturally heterogeneous fractured rock systems. These features include preferential flow patterns and fast flow paths, evidenced by direct field observations on flow (e.g., Salve, 2005), by indirect implications from fast chemical migration (e.g., Nativ et al., 1995), and by numerical simulation of unsaturated flow in heterogeneous fractured rock (e.g., Bodvarsson et al., 2003; Zhou et al., 2003). The conceptual understanding is that only a portion of connected fractures, referred to as active fractures, conduct water, while other connected fractures are bypassed and have no effects on global liquid flow. This understanding is quantitatively characterized in the active fracture model by introducing an additional parameter, fracture activity γ, to represent the fraction of active fractures in the framework of the van Genuchten model (van Genuchten 1980).

The active fracture model has been applied extensively to the site characterization of mountain-scale unsaturated flow at Yucca Mountain. The γ parameter has been calibrated using field data on ambient water saturation, potential, and pneumatic pressure. Indirect model validation was conducted by Liu et al. (2003) using field data on fracture-coating spatial distributions, which are consistent with the simulated spacing of active fractures derived from calibrated γ value. However a direct relationship between the γ parameter and the degree of rock-property heterogeneity, which causes preferential flow, has never been established.

In this study, numerical experiments on unsaturated flow in fractured rock, under the effects of small-scale heterogeneity, were used to derive the constitutive equations between effective capillary pressure, relative permeability and liquid saturation by specifying different infiltration rates at the top boundary. The physical meaning and dependence of the γ parameter on the degree of heterogeneity of fracture permeability was obtained through numerical experiments using different log fracture-permeability fields with varying correlation length and standard deviation.

2. MATHEMATICAL MODEL

In unsaturated fractured rock, fractures and the matrix are frequently considered as two overlapping continua with interaction of liquid flux at the fracture-matrix interface. We used this so-called dual-permeability model to simulate unsaturated flow in each of the two continua and mass exchange at the interfaces.

2.1. Unsaturated Flow Equations

The unsaturated flow in fractures and the matrix is written using Richards' equation (1931):

$$\frac{\partial \phi_f S_f \rho}{\partial t} = \frac{\partial}{\partial x_i}\left(k_f \frac{k_{rf}}{\mu} \rho \frac{\partial}{\partial x_i}\left(P_f + \rho g z\right)\right) - q_{fm}, \quad (1)$$

$$\frac{\partial \phi_m S_m \rho}{\partial t} = \frac{\partial}{\partial x_i}\left(k_m \frac{k_{rm}}{\mu} \rho \frac{\partial}{\partial x_i}\left(P_m + \rho g z\right)\right) + q_{fm}, \quad (2)$$

respectively, where subscripts *f* and *m* indicate the fracture and matrix continuum, respectively, ϕ is the porosity, S is the liquid saturation, ρ (kg m^{-3}) is the liquid density, k (m^2) is the permeability, k_r is the relative permeability of liquid, μ (Pa s) is the dynamic viscosity, P (Pa) is the liquid pressure, x_i (m, $i = 1, 2, 3$ in three dimensions) is the ith component of the Cartesian coordinate with z ($= x_3$) as the vertical coordinate (positive upward), t (s) is the time, and q_{fm} is the advective flux of liquid through the fracture-matrix interface from the fracture continuum to the matrix continuum per unit volume of fractured rock. The interface flux depends on the pressure gradient between the two continua, fracture saturation, and interface permeability. The interface permeability is generally approximated by the product of upstream relative permeability and matrix permeability.

2.2. Active Fracture Model

The active fracture model was developed by Liu et al. (1998), based on the van Genuchten model, to help solve the flow equations, Eqs. (1) and (2), in a closed form. In the van Genuchten model, liquid relative permeability and capillary pressure are nonlinearly related to water saturation under the assumption that liquid in different pores is at equilibrium status. The constitutive equations of the van Genuchten model have been extensively used in both porous media and fractured rock. The active fracture model was developed to effectively account for preferential-flow features in naturally heterogeneous fractured rock. In this model, effective liquid saturation (S_e^a), capillary pressure (P_c^a), and relative permeability (k_r^a) for active fractures are written in the form:

$$S_e^a = S_e^{1-\gamma} \quad (3a)$$

$$P_c^a = \alpha^{-1}\left(S_e^{(\gamma-1)/m} - 1\right)^{1-m} \quad (3b)$$

$$k_r^a = S_e^{(1-\gamma)/2}\left(1 - \left(1 - S_e^{(1-\gamma)/m}\right)^m\right)^2 \quad (3c)$$

where S_e is the effective liquid saturation ($S_e = S_f - S_{rf} / 1 - S_{rf}$) for the fracture continuum, S_f and S_{rf} are the fracture saturation and residual saturation, respectively, α^{-1} (Pa) is the fracture (characteristic) capillary strength, m is the fracture slope parameter, and γ, ranging from 0 and 1, is the fracture "activity" to represent fraction of active fractures in all connected fractures.

When $\gamma = 0$, the active fracture model degrades to the traditional van Genuchten model, and all connected fractures are active in conducting liquid flow. However, when $\gamma > 0$, only a portion of connected fractures conducts liquid flow, whereas other fractures are inactive for global flow. The γ parameter has been calibrated using field measurements on fracture geometries, fracture permeability, saturation, and pneumatic pressure. For example, a value of 0.41 was calibrated from fracture-coating spatial distributions when an indirect validation was conducted (Liu et al., 2003).

The active fracture model has been extensively applied to unsaturated flow and transport at Yucca Mountain. However, no direct model validation has been performed through field experiments. This may be because it is very difficult, if not impossible, to measure the effective values of saturation, capillary pressure and relative permeability over a large scale. Numerical experiments, on the other hand, can be easily conducted on unsaturated flow in fractured rock. Preferential flow patterns and fast flow paths can be obtained by simulating unsaturated flow with spatially varying fracture properties generated randomly (e.g., Birkholzer et al., 1999; Bodvarsson et al., 2003; Zhou et al., 2003).

3. NUMERICAL EXPERIMENTS

The numerical experiments conducted in this study include (1) simulation of unsaturated flow in a fractured rock system with randomly generated fracture-permeability fields, (2) upscaling of effective values of saturation, capillary pressure, and relative permeability over the entire domain using a flux-weighting method to focus on effects of active fracture zones, (3) derivation of domain-averaged

$\overline{k_r^a} - \overline{P_c^a} - \overline{S_e^a}$ constitutive equations with varying $\overline{S_e^a}$ values by changing infiltration rates at the top boundary, (4) calculation of the γ parameter based on the active fracture model and the constitutive equations derived from the numerical experiments, and (5) analysis of the dependence of the effective $\overline{k_r^a} - \overline{P_c^a} - \overline{S_e^a}$ constitutive equations and the γ parameter on the degree of heterogeneity of fracture permeability (k_f) by generating different k_f fields using varying correlation length and standard deviation of $\log_{10} k_f$ values.

3.1. Experiment Setup

As shown in Figure 1, a two-dimensional vertical cross section was employed as flow domain. The domain was 100 m wide in the horizontal direction and 100 m thick in the vertical direction. A uniform discretization of 0.5 m was used for both directions. Despite the relatively fine discretization, each grid element comprises several fractures and matrix blocks, due to the intense fracturing in the repository units at Yucca Mountain (with typical fracture spacings of a decimeter or less). Based on the fracture geometric data from the Yucca Mountain site, a dual-permeability mesh was generated. The mesh consists of 40,000 fracture elements, 40,000 matrix elements, one fracture element at the top, and one fracture element at the bottom boundary. The mesh also consists of a total of 200,000 connections for fracture–fracture, matrix–matrix, and fracture–matrix interactions (Pruess et al., 1999).

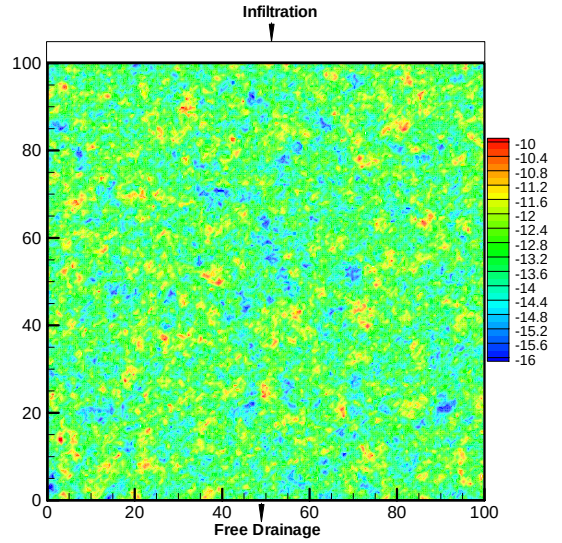

Figure 1. Numerical experiment setup with a generated random field of $\log_{10} k_f$ with standard deviation of 0.81 and correlation length of 1 m.

Liquid infiltration was specified at the top fracture element connected to the immediately underlying 200 fracture elements and 200 matrix elements. The spatial distribution of infiltration from the top boundary into the underlying elements depends on their permeability distribution. A higher permeability at an element produces a larger fraction of specified total infiltration rate into that element. This self-adjustable boundary condition is appropriate to represent the redistributed flow rate into the middle of a thick unsaturated zone, from rainfall events at the ground surface. The free-drainage condition under gravity only was specified at the bottom boundary by assuming negligible capillary force gradient. The vertical lateral boundaries were no-flow boundary.

The rock properties for the repository host horizon within the Topopah Spring welded Tuff (TSw) hydrogeologic unit at Yucca Mountain were used in this study. Specifically, the calibrated fracture and matrix properties of the TSw35 layer were used as model input (BSC, 2003). These rock-property values were calibrated in previous studies using a large number of field data on rock properties (e.g., matrix permeability and porosity), ambient flow conditions (e.g., matrix saturation and water potential), and field tests (e.g., pneumatic pressure and air permeability) (BSC, 2003; Zhou et al., 2003). Considering the scale of the numerical experiments, the drift-scale calibrated rock property values, representing layer-averaged mean values at a scale of 10 m or less, were used.

3.2. Random Fields of Fracture Permeability

Heterogeneity in fracture properties was introduced using spatially varying fracture permeability (k_f) and capillary strength (α_f^{-1}). The k_f random fields were generated using the Sequential Gaussian Simulator (SGSIM) in the GSLIB library (Deutsch and Journel, 1998), whereas the α_f^{-1} values were automatically scaled to the corresponding k_f values using the Leverett scaling.

3.2.1. Fracture permeability data

The generation of k_f random fields was based on the site-specific fracture permeability data obtained from air injection tests. Different data sources with different observation scales, from 0.3 m to 12 m, (i.e., the packer length for air-injection tests) were available. Considering the size of the numerical gridblocks, we used the small-scale air permeability data (i.e., 0.3m packer length) with hundreds of measurements obtained in several boreholes in two niches excavated in a tunnel (BSC, 2003). In each

borehole, approximately 30 data points were obtained with continuous uniformly-spaced packer intervals. The data obtained in Niche 3107 (which is located in less intensely fractured rock) and Niche 4788 (which is located in highly fractured rock), assumed as mutual independent samples from the same population, were used for deriving statistic properties of the spatially varying fracture permeability. Note that all the data are pre-excavation data, which represent the undisturbed rock conditions before excavation of nearby niches.

As shown in Figure 2, the measured fracture permeability (m^2) varies over five orders of magnitude, with a mean of -13.16 and a standard deviation of 0.81 for $\log_{10} k_f$. The fracture permeabilities obey the lognormal distribution, which is consistent with many other conclusions on permeability distribution in porous media. The covariance function and variogram obtained for each borehole indicate that a weak correlation exists, with a correlation scale from 0.6 m to 1.2 m. Because all data in each borehole were collected in one direction only, an isotropic correlation length was assumed in this study.

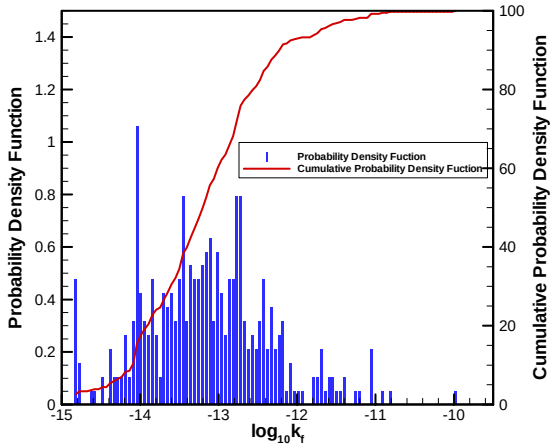

Figure 2. Probability and cumulative probability density functions of measured fracture air permeabilities obtained under pre-excavation conditions at Yucca Mountain.

3.2.2. Generation of fracture permeability fields

To represent the strong spatial variability of fracture permeability discussed above, we generated a random field of fracture permeability using the SGSIM scheme. As the base case for the following sensitivity analysis, we used the statistic mean ($\mu_{\log_{10} k_f} = -13.16$) and standard deviation ($\sigma_{\log_{10} k_f} = 0.81$) derived from the data. The correlation scale of 1.0 m ($\lambda = 1\ m$) on average was used, with the exponential covariance model. In the generation process, we first generated the $\log_{10} k_f$ field based on the normalized Gaussian distribution and the given correlation length; then we transformed the generated values back to the k_f values. The generated fracture permeability field was bounded by ± 3.0 orders of magnitude around the geometric mean. The geometric mean and variance of the generated field was very close to the input parameters with less than 2% errors. This indicates that the generated random field can be used to represent the small-scale heterogeneity in the field, and enables the comparison of flow simulation results between heterogeneous and homogeneous scenarios.

In addition to the base case, we also generated one additional random field of fracture permeability, with a correlation length of 5 m and a standard deviation of 1.5. This case was used for analyzing the dependence of effective (domain-averaged) constitutive equations and the γ parameter on the degree of heterogeneity of fracture-rock properties.

3.3. Upscaling

With the generated fracture permeability field, the specified values of all other mean rock properties, and a specified infiltration rate at the top boundary, a steady-state unsaturated flow field was simulated using the TOUGH2 code (Pruess et al., 1999), a general-purpose reservoir simulator for multi-dimensional coupled fluid and heat flow of multiphase, multi-component fluid mixtures in porous and fractured media.

The flow simulations give spatially-varying saturation values, as well as capillary pressure and relative permeability values based on the local-scale van Genuchten model parameters used in this study. To focus on the effects of active, water-conducting fracture zones, we used a flux-weighting method to obtain domain-averaged effective values from their local-scale values:

$$\overline{S_e^a} = \sum_{j=1,n} F_{vj} S_{ej} \Big/ \sum_{j=1,n} F_{vj} \ , \qquad (4a)$$

$$\overline{P_c^a} = \sum_{j=1,n} F_{vj} P_{cj} \Big/ \sum_{j=1,n} F_{vj} \ , \qquad (4b)$$

$$\overline{k_r^a} = \sum_{j=1,n} F_{vj} k_{rj} \Big/ \sum_{j=1,n} F_{vj} \ , \qquad (4c)$$

where F_{vj} is the vertical flux at the *j* element, and *n* is the total number of fracture elements. The reason for using the vertical flux as the weighting factor is because the unsaturated flow is gravity-dominated,

and vertical flux is much larger than horizontal flux. (Note that the effective values were calculated for fracture elements only.) This flux-weighting upscaling method is different than the arithmetic averaging method. In the latter, the effective values were obtained through the simple arithmetic averaging, as Zhou et al. (2002) derived the effective constitutive equations in two-phase flow conditions in porous media. The arithmetic averaging method was also used here for comparison with the flux-weighting method.

The upscaled $\overline{P_c^a}$ and $\overline{k_r^a}$ values with respect to $\overline{S_e^a}$ were considered as one data pair for deriving domain-averaged, effective $\overline{P_c^a} - \overline{k_r^a} - \overline{S_e^a}$ constitutive equations. To obtain such constitutive equations, seven unsaturated flow fields were obtained by varying infiltration rates specified at the top boundary, from 0.5 mm/year (small overall saturation) to 5,000 mm/year (large overall saturation). The obtained effective constitutive equations represent the effects of local-scale heterogeneity and preferential-flow patterns.

For comparison with the upscaled, domain-averaged constitutive equations, we also simulated unsaturated flow in a homogeneous fractured rock system, whose fracture permeability was the mean value of the generated k_f random field. The derived constitutive equations represent the domain-averaged ones without preferential flow and heterogeneity, which are identical to the local-scale constitutive equations used for the numerical modeling.

4. RESULTS AND DISCUSSION

4.1. Base Case Scenario

Figure 3 shows the spatial distribution of simulated liquid saturation, capillary pressure, and vertical liquid flux in the fracture continuum, in the case of an infiltration rate of 500 mm/year specified at the top boundary. High fracture flux occurs within three major fracture zones, between which saturation is relatively small and fluxes are comparably low. Within each of the three fast flow fracture zones, relatively higher flux occurs in the center, with smaller fluxes on the sides. The vertical flux varies over two orders of magnitude. These simulation results indicate that numerical experiments can be used to produce preferential-flow features.

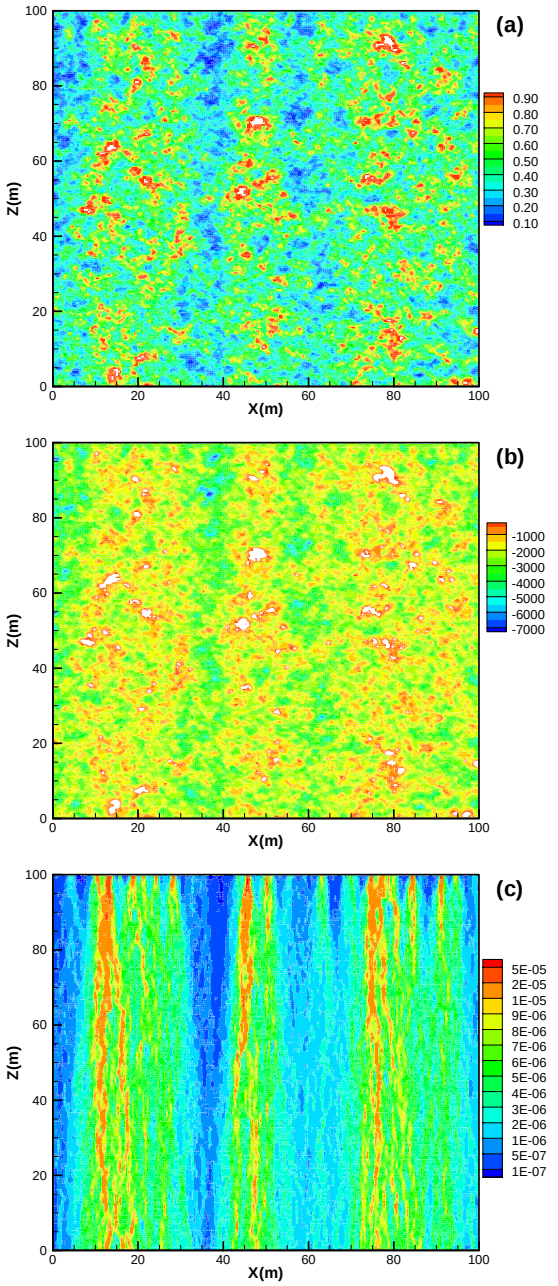

Figure 3. (a) Liquid saturation, (b) capillary pressure (Pa), and (c) vertical flux (kg/s) in the fracture continuum simulated using the spatially varying log fracture permeability with $\sigma_{\log_{10} k_f} = 0.81$ *and* $\lambda = 1\ m$.

A higher vertical flux generally corresponds to a higher fracture saturation. Accordingly, three fracture zones of higher saturation, separated by two fracture zones of lower saturation, can be seen clearly. The formation of these wet and dry fracture zones depends mainly on the spatial distribution of liquid

flux into the model domain through the top boundary, because the unsaturated flow is dominated by gravity. In addition to the large-scale high and low saturation patterns, the liquid saturation field also exhibits local-scale variations within each of these fracture zones. The local-scale variations correlate well with the generated $\log_{10} k_f$ field (see Figure 1). A higher fracture permeability generally corresponds to a lower saturation. This is because the effective permeability (product of relative permeability and intrinsic permeability) at any given element should be close to that of the underlying element, in the case of dominant gravity-driven flow. As a result, unlike the vertical flux, high saturation areas within a wet fracture zone are not continuous throughout the entire domain thickness. The same conclusion can be drawn for the local-scale capillary pressure.

Figure 4 shows the resulting effective capillary pressure and relative permeability relationships averaged over the flow domain. The domain-averaged $\overline{k_r^a} - \overline{P_c^a} - \overline{S_e}$ curves are different from the local-scale $k_r - P_c - S_e$ curves of the homogeneous case. The effective relative permeability values are always higher than their homogeneous counterparts for the same $\overline{S_e}$ or S_e values (or the same infiltration rate specified at the top boundary). Note that $\overline{S_e}$ is the mean effective liquid saturation for the entire domain calculated using the arithmetic averaging method. This indicates that most of water migrates downward within high-flux fracture zones where water saturation is generally high. The higher water saturation within flow-focused areas results in higher relative permeability since the same slope parameter (m) was used. The deviation of the effective relative permeability curve from the local-scale one observed here is consistent with that predicted by the active fracture model.

The effective capillary pressure curve is also different from the local-scale curve, although the difference is not significant. The effective capillary pressure is higher than the local-scale value when the effective saturation is small (e.g., $\overline{S_e} < 0.6$). In the case of higher saturation, the effective capillary pressure is slightly smaller than the local-scale value. This observation through numerical experiments is contradictory to that of the active fracture model. In that model, capillary pressure in active fractures is always smaller than that predicted by the traditional van Genuchten model (i.e., $\gamma = 0$). Such a difference may be attributed to the spatially varying capillary strength (α_f^{-1}), which is negatively correlated to fracture permeability. This means that within the fracture zones of high liquid flux and saturation, there may be some areas having high capillary pressure resulting from high α_f^{-1} values, in spite of their relatively large local saturation.

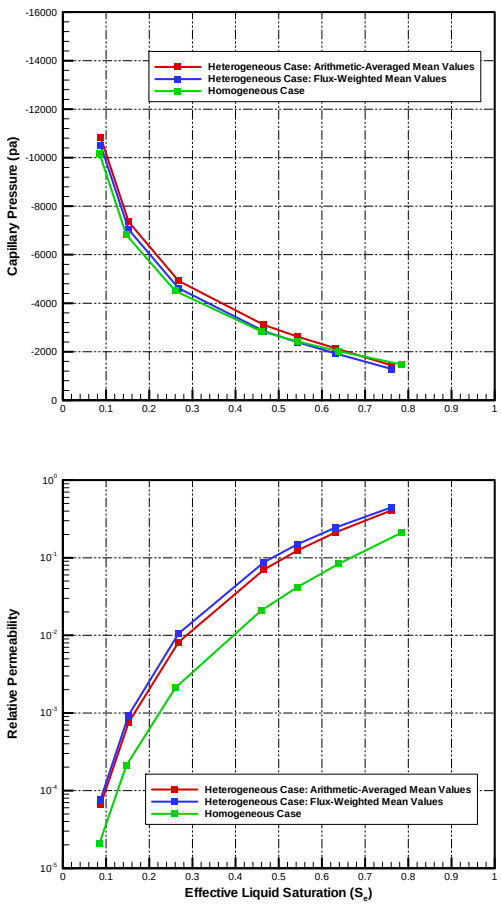

Figure 4. Comparison of effective capillary pressure and relative permeability, as functions of mean effective water saturation, for a fractured rock system between homogeneous and spatially varying fracture permeability with $\sigma_{\log_{10} k_f} = 0.81$ *and* $\lambda = 1\ m$.

In the case of not very strong fracture-permeability heterogeneity, no significant difference is observed between the effective constitutive curves obtained using the flux-weighting method and the arithmetic averaging method, although the calculated effective saturations by the two methods are different for a given infiltration rate specified at the top boundary.

Figure 5 shows the change of the calculated γ parameter with the mean liquid saturation ($\overline{S_e}$). Note that the γ values were calculated using Eq. (3c), and simulated $\overline{S_e}$ and $\overline{k_r^a}$ values. The γ parameter

varies from 0.02 for the mean liquid saturation of 0.08 to 0.14 for $\overline{S_e} = 0.76$. The dependence of the γ parameter on liquid saturation observed here is different from the assumption in the active fracture model that the constant "activity" parameter can be used for the entire saturation range from 0 to 1. Note that this difference may be attributed to the completely different concept used in the active fracture model and the numerical experiments in this study. In our numerical experiments, capillarity in the fracture continuum tends to be at equilibrium conditions between different elements within high-flux fracture zones as in the van Genuchten model. In contrast, the active fracture model presumes gravity-dominated, nonequilibrium, preferential liquid water flow in fractures (Liu et al., 1998, p2635).

As shown in Figures 3 and 4, significant preferential flow patterns and their effects on the domain-averaged, effective constitutive equations were observed. Higher flow rates occur within isolated active fracture zones. Therefore, the effects of preferential flow features should be considered in the mathematical modeling, as done in the active fracture model.

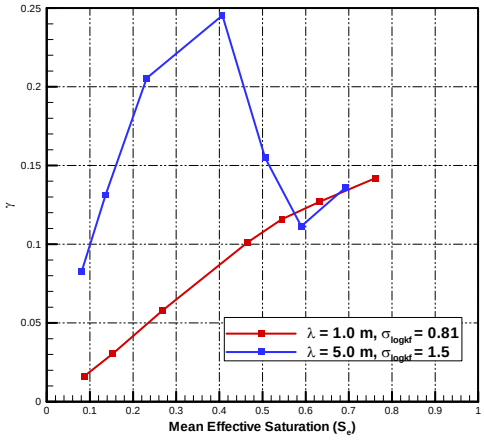

Figure 5. Dependence of the estimated λ parameter of the Active Fracture Model on mean effective water saturation in the two numerical experiments.

4.2. Dependence on Degree of Heterogeneity

Figure 6 shows the domain-averaged constitutive curves for effective capillary pressure and relative permeability with respect to liquid saturation in the case of $\sigma_{\log_{10} k_f} = 1.50$ and $\lambda = 5\ m$. With the increase in the degree of fracture-permeability heterogeneity, the separation between the domain-averaged, effective curves and their local-scale curves increases. The more heterogeneous the fractured rock is, the more dominant are the preferential-flow features. In the stronger heterogeneity case, the difference in the domain-averaged constitutive curves obtained by the flux-weighting and the arithmetic averaging method is apparent. In particular, the effective saturation calculated for each infiltration rate is significantly different.

The "activity" parameter is higher than its value for the base case, indicating fewer factures or less area of fracture zones are active in conducting water flow (see Figure 5).

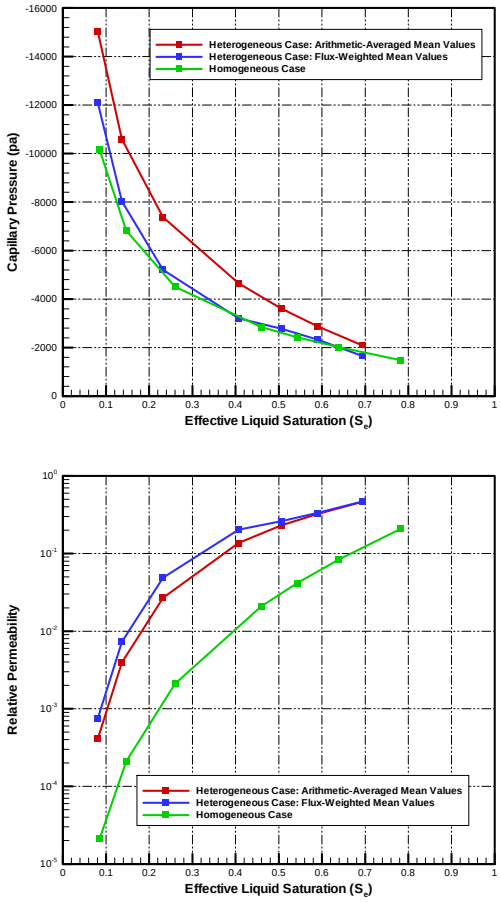

Figure 6. Comparison of effective capillary pressure and relative permeability, as functions of mean effective water saturation, for a fractured rock system between homogeneous and spatially varying log fracture permeability with $\sigma_{\log_{10} k_f} = 1.50$ and $\lambda = 5\ m$.

5. CONCLUSIONS

The active fracture model has been extensively applied to modeling flow and transport in unsaturated fractured rock at Yucca Mountain. It focuses on preferential flow within active, water-conducting fractures, whereas the effects of non-active, bypassed dry fractures are excluded. To validate the active fracture model, a methodology for upscaling local-scale constitutive equations on capillary pressure, relative permeability, and saturation to domain-averaged counterparts was developed. Numerical experiments on unsaturated fracture flow in heterogeneous fractured rock systems were used to capture the preferential-flow features. The flux-weighting upscaling method was employed to focus on the effects of active fracture zones on large-scale flow.

The results of numerical experiments demonstrate that domain-averaged constitutive curves on effective capillary pressure, relative permeability, and liquid saturation are different from the local-scale curves used for a homogeneous fractured rock system. A higher relative permeability was obtained for the heterogeneous scenarios, which is consistent with that predicted by the active fracture model. A slightly higher effective capillary strength was also observed, which is contrary to the active-fracture–model prediction. This contradiction may be attributed to the fact that in the numerical experiments, capillarity tends to be at equilibrium conditions as in the van Genuchten model, whereas the active fracture model presumes gravity-dominated, nonequilibrium, preferential liquid water flow in fractures.

The fracture "activity" parameter in the active fracture model was observed to change with liquid saturation. Moreover, this parameter increases with increasing degree of fracture-permeability heterogeneity. Such finding helps us to link the fracture "activity" parameter to fracture rock characteristics (in particular statistical properties and heterogeneity). In a homogenous fracture rock system, all fractures are active in conducting liquid flow because each fracture is equally important. In a heterogeneous fracture rock, only a portion of connected fractures participate in global water flow. Thus, in a fracture rock system with stronger heterogeneity, more profound preferential flow occurs and less fracture zones or areas are active.

REFERENCES

Birkholzer, J.T., G. Li, C.-F. Tsang, Y. Tsang, Modeling studies and analysis of seepage into drifts at Yucca Mountain, J. Contam. Hydrol., 38, 349–384, 1999.

Bodvarsson, G. S, Y. S. Wu, and K. Zhang, Development of discrete flow paths in unsaturated fractures at Yucca Mountain, *J. Contam. Hydrol*., 62–63, 23-42, 2003.

Liu, H. H., C. Doughty, G. S. Bodvarsson, An active fracture model for unsaturated flow and transport in fractured rocks, *Water Resour. Res*., 34(10), 2633–2646, 1998.

Liu H. H., G. Zhang, G., and G. S. Bodvarsson, The active fracture model: its relation to fractal flow patterns and an evaluation using field observations, *Vadose Zone J*, 2: 259–269, 2003.

Nativ, R., E. Adar, O. Dahan, M. Geyh, Water recharge and solute transport throughthe vadose zone of fractured chalk under desert conditions, *Water Resour. Res*., 31(2), 253–261, 1995.

Pruess, K., On water seepage and fast preferential flow in heterogeneous, unsaturated rock fractures, *J. Contam. Hydrol*., 30, 333–362, 1998.

Pruess, K., C. M. Oldenburg, and G. Moridis, *TOUGH2 User's Guide, Version 2.0*, Report LBNL-43134, Lawrence Berkeley National Laboratory, Berkeley, Calif., 1999.

Richards, L.H., Capillary conduction of liquids through porous mediums, *Physics*, 1, 318–333, 1931.

Salve, R., Observation of preferential flow during a liquid release experiment in fractured welded tuffs, *Water Resour. Res*. 41, W09427, doi:10.1029/2004WR003570, 2005.

van Genuchten, M.T., A closed form equation for predicting the hydraulic conductivity of unsaturated soils, *Soil Sci. Soc. Am. J*., 44, 892-898, 1980.

Zhou, Q., H-H Liu, G. S. Bodvarsson, C. M. Oldenburg, Flow and transport in unsaturated fractured rock: effects of multiscale heteroeenity of hydrogeologic properties, *J. Contam. Hydrol*., 60, 1-30, 2003.

Zhou, Q., L. W. Gelhar, B. Jacobs, Comparison of field-scale effective properties of two-phase flow in heterogeneous porous media obtained by stochastic analysis and numerical experiments. In Findikakis A.N. (Ed.), Proceedings of the international groundwater symposium on bridging the gap between measurements and modeling in heterogeneous media, Berkeley, California, 2002.